

Behavior of Railway Cars in Running (Report 3)

— Simulation on Derailment —

Seinosuke ARAI

Abstract

The safety of railway cars is checked mainly through running test, with full size cars under various conditions of car elements and track irregularities. In parallel to these surveys, here introduced the simulation method of car motion with an electronic computer, applying the data of the above-mentioned running tests. The simulation technique is now playing an important role to make clear the cause of derailment of railway cars in train accidents.

Nomenclature

Notation	Unit	Definition
a	m	half length of wheel base
a_1	m	constant related to an amplitude of lateral vibratory displacement
a_2	m	constant related to an amplitude of lateral vibratory displacement
b	m	half distance between contact points of wheel treads and rails in the lateral direction
b_1	m	half spacing of suspension mountings for a wheelset
c_x	kgf·s/m	damping coefficient in the longitudinal direction (conversion to bearing spring position, for an axle)
c_y	kgf·s/m	damping coefficient in the lateral direction (for an axle)
c_z	kgf·s/m	damping coefficient in the vertical direction (conversion to bearing spring position, for an axle)
F	kgf	tangential force; frictional force
F_{y1}	kgf	frictional force of a front wheelset in the lateral direction
F_{y2}	kgf	frictional force of a rear wheelset in the lateral direction
g	m/s ²	=9.8; acceleration of gravity
h	m	height of body center of gravity above the middle of bearing spring
i_w	m	$=\sqrt{I_w/m_w}$; radius of gyration of wheelset in yaw
i_x	m	$=\sqrt{I_{Bx}/m_B}$; radius of gyration of half body in roll
i_z	m	$=\sqrt{I_{Bz}/m_B}$; radius of gyration of half body in yaw
k_r	kgf/m	longitudinal supporting stiffness of an axle
k_y	kgf/m	lateral supporting stiffness of an axle
m_B	kgf·s ² /m	half mass of car body
m_w	kgf·s ² /m	mass of a wheelset
Q_{L1}	kgf	lateral force applied to front left wheel by rail
Q_{L2}	kgf	lateral force applied to rear left wheel by rail
Q_{R1}	kgf	lateral force applied to front right wheel by rail
Q_{R2}	kgf	lateral force applied to rear right wheel by rail
Q_{1L1}	kgf	longitudinal force applied to front left wheel by rail
Q_{1L2}	kgf	longitudinal force applied to rear left wheel by rail
Q_{1R1}	kgf	longitudinal force applied to front right wheel by rail
Q_{1R2}	kgf	longitudinal force applied to rear right wheel by rail
R	m	radius of curvature of curved track
r	m	radius of wheel tread circle
r'	m	height of bearing spring above rail tread

Received October 20, 1982

Notation	Unit	Definition
S_1	rad	relative angular displacement between body and front wheelset in yaw
S_2	rad	relative angular displacement between body and rear wheelset in yaw
t	s	time
V	km/h	forward car speed
v	m/s	forward car speed
X_1	m	relative displacement between body and front wheelset at bearing spring position
X_2	m	relative displacement between body and rear wheelset at bearing spring position
x		longitudinal axis; a variable
y		lateral axis
y_1	m	lateral displacement of front wheelset; lateral displacement of wheelset (mode 1)
y_2	m	lateral displacement of rear wheelset; lateral displacement of wheelset (mode 2)
z		vertical axis
α_1	rad/s	real part of characteristic number
α_2	rad/s	real part of characteristic number
β		scale factor of analogue computation
ζ	m	$=h\phi$
θ	rad	an angular variable
ξ	m	$=a\psi$
ϕ	rad	angular displacement in roll
ϕ_B	rad	angular displacement of body in roll
ψ	rad	angular displacement in yaw
ψ_B	rad	angular displacement of body in yaw
ψ_1	rad	angular displacement of front wheelset in yaw
ψ_2	rad	angular displacement of rear wheelset in yaw
ω_1	rad/s	imaginary part of characteristic number; angular frequency
ω_2	rad/s	imaginary part of characteristic number; angular frequency

Simulation of Lateral Motion of a 2-Axle Railway Car¹⁾

1. The lateral motion characteristics of a 2-axle car

An example of the characteristics for a 2-axle railway car in lateral is shown in Fig. 1.1. If a running speed is fixed, α_1 , ω_1 , α_2 , ω_2 can be read from the figure. The followings are the fundamental expressions on lateral motion. $\alpha > 0$ means divergent or unstable and $\alpha < 0$ means convergent or stable at the concerned speed.

$$y_1 = a_1 e^{\alpha_1 t} \cos \omega_1 t$$

$$y_2 = a_2 e^{\alpha_2 t} \cos \omega_2 t$$

There are two stable ranges, high speed range and low speed one. We call them the upper stable range and the lower stable range, respectively. The double link suspension device was developed to make use the upper stable range. Thus the operation speed of 2-axle freight car with double link suspension was able to raise to 75 km/h.

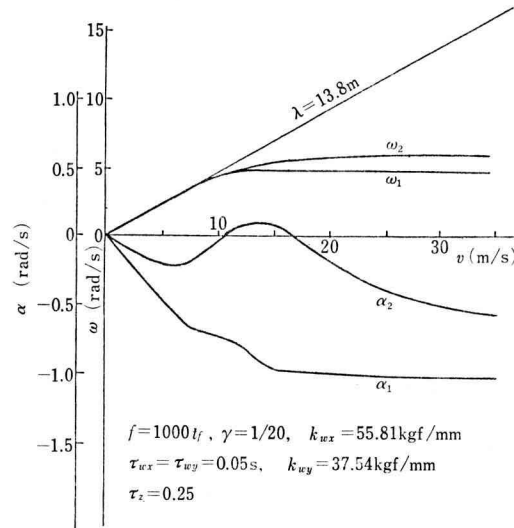


Fig. 1.1 Vibrational characteristics to car speed for a 2-axle railway car (principal modes)

2. Method of simulation

There were relatively many cases of 2-axle railway car derailment, which was considered to occur by the interaction of various conditions. The phenomenon of such derailment is hard to make clear with an exact analytical way, but the effect of various factors and their combination has been clarified step by step by simulation methods with an electronic computer, which has made great progress in recent years.

The method here described is a simulation with a hybrid computer program of a 2-axle railway car motion in running on track with irregularities in lateral or/and in cross level. Wheel side thrust, wheel load and their ratio (Q/P or derailment factor) are recorded on oscillograph paper in time base. This simulation can be applied to investigate how the conditions of railway cars and tracks affect on derailment due to off-loading of wheels or due to generating of wheel side thrust in various ways.

2.1 Adoption of a hybrid computer

A hybrid computer is a combination of analogue computer, digital computer and their linkage. Each computer's merits are effectively used.

There are two methods of hybrid computation, that is, analogue part and digital part compute in series and in parallel. The former is the alternative computation method, that is, after ending analogue computation, digital part compute in series using the results of the analogue one, and the result of digital execution are used in the following analogue computation. The latter is the method that analogue and digital computations execute simultaneously, and data are continuously transmitted with each other. In recent years,

it is a fact that the analogue computer is looked poor due to the development of large-sized and high-speed digital computer, but the analogue computation exceeds digital one in execution time for simultaneous differential equations with time as an independent variable, because the differential equations are solved in parallel. It is faster than digital computer to calculate high order equations, such as multi-degrees-of-freedom of motion in dynamics. The difference of time consumption becomes significant especially many cases with various parameters have to be executed.

A hybrid computer is effectively used in the field containing both simultaneous differential equations and algebraical calculations. The system of railway car motion fits this condition. Table 2.1 is an outline of the hybrid computer for this simulation.

2.2 Representation of a railway car

Lateral, yawing and rolling motions are taken into consideration for car body motion,

Table 2.1 Composition of hybrid computer

Analogue computer		
type: Hitachi ALS-2000		
operational amplifier	total	120 sets
integrator		40 sets
adder		40 sets
sign changer		40 sets
potentiometer	total	200 sets
manual pot.		20 sets
servo setting pot.		180 sets
multiplier		8 sets
output indicator	total	3 sets
pen-writing oscillograph (8 elements)		1 set
x-y recorder		1 set
oscilloscope		1 set
Digital computer		
type: Hitachi CLOAP-2000E		
memory size	16 KW (1W=18 bits)	
memory cycle-time	2 μ s	
addition and subtraction	6 μ s (single words)	
	9 μ s (double words)	
input-output instrument	total	3 sets
universal input-output typewriter		1 set
photo paper-tape reader		1 set
high-speed puncher		1 set
DA converter		16 sets
AD converter		16 sets

and vertical, longitudinal and pitching motions are neglected for their little affection on derailment and are reserved for another study occasion.

The dynamic model of a 2-axle railway car consists of seven degrees-of-freedom; three (lateral, yawing, rolling) for the body, two (lateral, yawing) for each wheelset. Its motion is expressed with analogue computation. Forces acting to the car are those produced at the contact point of rail and wheel, gravitational, etc., and are treated by digital computation. Figure 2.1 shows its outline. In running the car on a curved track, centrifugal force or turning moment at transition parts from or to straight track are also introduced.

Digital part of a hybrid computer can do preparatory works such as setting potentiometers of analogue part, or general control of operation. The results of computation are recorded on oscillograph paper. The necessary input data for computation are taken mainly from digital part, except such part as manual setting of potentiometers.

The car motion in this simulation is generated by irregularities of track. These irregularities are set in the digital part as track data, and various car motions are shown by the given forms of irregularities and by the car model characteristics.

When the execution starts, digital part reads the information on car model through AD converter and then computes the forces produced at wheel tread, involving flange part, on the relation with the track irregularities at that position and moment. The computation results are transmitted to analogue part through DA converter.

It takes 20 ms for one cycle of the digital computation. As the computation is

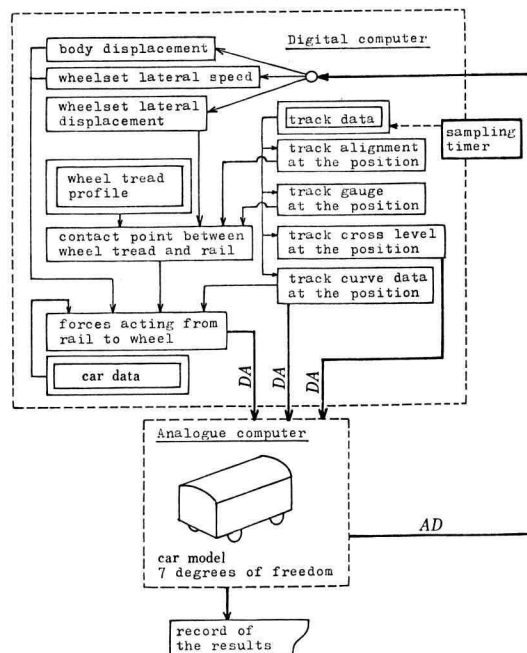


Fig. 2.1 Outline of simulation with hybrid computer

$$2m_B \ddot{y}_B = k_y(X_1 + X_2) + c_y(\dot{X}_1 + \dot{X}_2) + F_{y1}(X_1) + F_{y2}(X_2) \quad (2.5)$$

$$2m_B \ddot{\psi}_B = k_y a(X_1 - X_2) + c_y a(\dot{X}_1 - \dot{X}_2) + aF_{y1}(X_1) - aF_{y2}(X_2) \\ + k_x b_1^2(S_1 + S_2) + c_x b_1^2(\dot{S}_1 + \dot{S}_2) \quad (2.6)$$

$$2m_B \ddot{\phi}_B = k_y h(X_1 + X_2) + c_y h(\dot{X}_1 + \dot{X}_2) + hF_{y1}(X_1) + hF_{y2}(X_2) \\ + k_x b_1^2(P_1 + P_2) + c_x b_1^2(\dot{P}_1 + \dot{P}_2) + b_1 F_{x1}(P_1) + b_1 F_{x2}(P_2) \\ - 2m_B g \{y_B - (y_1 + y_2)/2\} \quad (2.7)$$

where,

$$X_1 = y_1 - y_B - a\psi_B - h\phi_B - r'\phi_1$$

$$X_2 = y_2 - y_B + a\psi_B - h\phi_B - r'\phi_2$$

$$S_1 = \psi_1 - \psi_B, \quad S_2 = \psi_2 - \psi_B$$

$$P_1 = \phi_1 - \phi_B, \quad P_2 = \phi_2 - \phi_B$$

F_{y1} , F_{y2} , F_{x1} , F_{x2} represent frictional forces and $F_{y1}(X_1)$ indicates a function of X_1 . These forces change with hysteresis and elasticity against displacement like Fig. 2.3.

(2.1), (2.2) are the equations of motion for front wheelset, (2.3), (2.4) are that for rear wheelset, and (2.5), (2.6), (2.7) are that for car body. The last term of equation (2.7) indicates the rolling moment produced by the gravitational force multiplied by the lateral displacement of the gravity center of car body. ϕ_1 , ϕ_2 represent the irregularities of cross level of track at the position under the front axle and the rear axle, respectively.

Details for analogue computation are described on Appendix I.

The forces, transmitted from rail to wheel, are obtained by the conditions of contact due to relative position of rail and wheel tread. To simplify the program, the following assumptions are taken.

- (1) Rails are rigid and fixed.
- (2) Wheel contacts rail at one point.

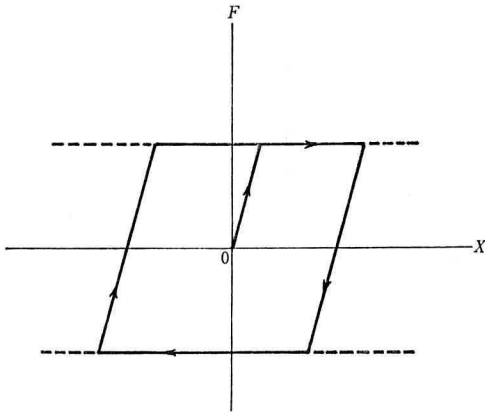


Fig. 2.3 Frictional force with elasticity in series

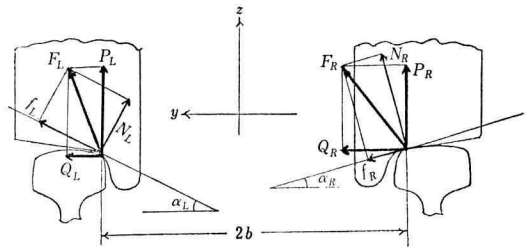


Fig. 2.4 Force acting to wheel tread

Forces acting between rail and wheel are shown in Fig. 2.4 where F is a force from rail to wheel, P is a wheel load (upward is positive), Q is a side thrust of wheel (positive direction is the same as y), α is an angle between level surface and tangential plane at the contact point of rail and wheel, N is a normal force and f is a tangential force. Subscripts L and R represent left wheel and right one, respectively (Fig. 2.4 is the view from rear side).

The force F is divided into wheel load P and wheel side thrust Q , x -component is neglected here, and at the same time it is divided N and f , creep force or frictional force. The following relations, therefore, hold among these forces.

For left wheel:

$$f_L = Q_L \cos \alpha_L + P_L \sin \alpha_L \quad (2.8)$$

$$N_L = P_L \cos \alpha_L - Q_L \sin \alpha_L \quad (2.9)$$

For right wheel:

$$f_R = Q_R \cos \alpha_R - P_R \sin \alpha_R \quad (2.10)$$

$$N_R = P_R \cos \alpha_R + Q_R \sin \alpha_R \quad (2.11)$$

From (2.8),

$$Q_L = -P_L \tan \alpha_L + f_L / \cos \alpha_L \quad (2.12)$$

Substituting to (2.9),

$$N_L = P_L / \cos \alpha_L - f_L \tan \alpha_L \quad (2.13)$$

From (2.10) and (2.11), in the same manner,

$$Q_R = P_R \tan \alpha_R + f_R / \cos \alpha_R \quad (2.14)$$

$$N_R = P_R / \cos \alpha_R + f_R \tan \alpha_R \quad (2.15)$$

Forces on tangential plane are considered to follow the creep theory. Representing x -component of the creep force as Q_1^0 and y -component as Q_2^0 , the following formulas hold:

$$\left. \begin{aligned} Q_{1L}^0 &= f_1(b\dot{\psi}/v + \Delta r/r) \\ Q_{1R}^0 &= -f_1(b\dot{\psi}/v - \Delta r/r) \end{aligned} \right\} \quad (2.16)$$

$$\left. \begin{aligned} Q_{2L}^0 &= -f_2(\dot{y}/v - \psi)/\cos \alpha_L \\ Q_{2R}^0 &= -f_2(\dot{y}/v - \psi)/\cos \alpha_R \end{aligned} \right\} \quad (2.17)$$

where f_1 is creep coefficient in x direction, f_2 is one in y direction, and Δr is the increase of radius of wheel at rail-wheel contact point followed by lateral displacement of wheelset. The signs of Q_{1L} , Q_{1R} and Q_{2L} , Q_{2R} are oriented same as x and y , respectively.

The tangential force is the same as creep force when it is small, but as its magnitude increases, it gradually changes to sliding frictional force between wheel tread and rail. The actual force Q is assumed to be given by the following formula, where F_μ and Q^0 mean frictional force and creep force, respectively:

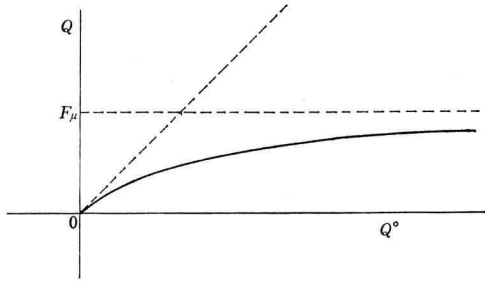
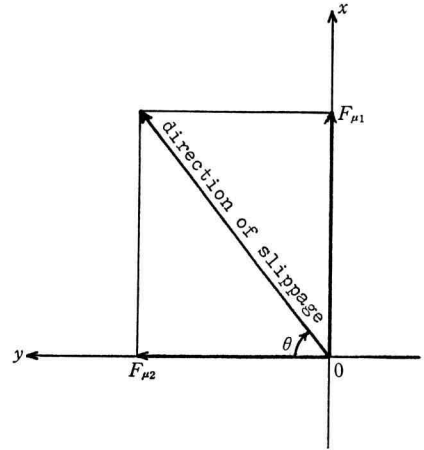
Fig. 2.5 Relation between Q° and Q 

Fig. 2.6 Relation between creep rate and the direction of slippage

$$1/Q = 1/F_\mu + 1/Q^\circ \quad (2.18)$$

This relation is shown in Fig. 2.5.

Creep force is regarded to produce independently in x direction and in y direction, whereas frictional force acts in the direction of slippage. Representing creep rate in x direction as α_1 , and one in y direction as α_2 , where creep rate meaning relative speed of wheel to rail divided by wheelset advancing speed.

Figure 2.6 shows the composition of slippage. Denoting angle θ as in the figure, in frictional range, the following formulas hold:

$$F_{\mu 1} = \mu N \sin \theta \quad (2.19)$$

$$F_{\mu 2} = \mu N \cos \theta \quad (2.20)$$

where, $F_{\mu 1}$ is frictional force component in x direction, $F_{\mu 2}$ is in y direction, and μ is a sliding frictional coefficient. N is a normal force and though it is expressed as (2.13), (2.15), the following simplified formulas are deduced:

$$N_L = P_L / (\cos \alpha_L) \quad (2.21)$$

$$N_R = P_R / (\cos \alpha_R) \quad (2.22)$$

where relative errors are considered small for large value of P .

Assuming the relation (2.18) holds on each of the x and y components,

$$1/Q_1 = 1/F_{\mu 1} + 1/Q_1^\circ \quad (2.23)$$

$$1/Q_2 = 1/F_{\mu 2} + 1/Q_2^\circ \quad (2.24)$$

The hybrid computation of simulation is carried out like a loop as shown in Fig. 2.1. The forces applied to wheel tread are calculated at digital part, that is:

- (1) Input the data on car motion from the analogue part through AD converter.

- (2) The input data are combined with the data on track irregularities of the points where the wheelsets of car are passing, and the forces acting to wheel tread are calculated.
- (3) The force is transmitted back to the analogue part of car model through DA converter.

The digital computation cycle time is desirable as short as possible in view of accuracy and length of execution time, but it takes about 20 ms or less, which is equivalent 2 ms of real time as the time scale of analogue computation is 10 times long. This delay of time results error in computation, but that is not so problematic against the phenomenon 20 Hz or so.

Details for hybrid computation are described on Appendix II.

2.3 Representation of a track

The track data to be provided are the irregularities of right side rail alignment (y_R), of gauge width (G_A) and of cross level (ϕ). These three kinds of irregularity can be obtained from measurement with track inspection car. The record of the measurement is called Maya-chart, where Maya is a name of railway car type. Each of y_R , G_A and ϕ along the distance of 300 m, are given by a folded line fixed within 150 points, because of the limitation by digital memory capacity.

The reason why the track data are given by distance base is that Maya-chart is recorded by distance base and also it is advantageous for varying car speed at simulation execution.

As it is laborous to make the folded lines with hand, a computer program is provided. The desirable folded lines must satisfy the following conditions:

- (1) The character of original wave form is well expressed, especially the peak values are almost equal.
- (2) The number of segments is as small as possible within a given deviation from original values.

In case of expressing an original wave with a folded line, it is considered that a method to minimize the mean value or the mean square of the deviation from the original wave, but in this case weight is given to large absolute values aparting from zero line, so that the peak values are remained.

In considering these conditions, an algorithm that folded points and peak points of wave form are connected one by one with straight segments is thought to be a good one, and the following method was developed.

At first an index value G is fixed properly. Supposing that a wave form $y(x)$ is given as Fig. 2.7, a beginning point $A(x_1, y_1)$ and a near point $B(x_2, y_2)$ are chosen. An arbitrary point $C(x_0, y_0)$ is taken on a curved line AB . The length of the segment CC' which is parallel to y axis in Fig. 2.7, is,

$$Z = |y_0 - y_1 - (y_2 - y_1)(x_0 - x_1)/(x_2 - x_1)| \quad (2.25)$$

After finding out Z_{\max} , for point C at a certain position on the curved line AB , the

point C corresponding to Z_{\max} is newly named as point C .

Letting:

$$Z_o = Z_{\max} \quad (2.26)$$

and going apart B from A towards the x positive direction, the value of Z_o may increase gradually. When Z_o reaches G at the first time, that is,

$$Z_o \geq G \quad (2.27)$$

C at that point is regarded as "a folded point", and renaming the C as new A , the folded points can be obtained one by one. The smaller the value of G is given, the more the number of points obtained. So by changing the value of G variously, the desirable set of points can be obtained as simulated wave form of the original one. An example with this method is shown in Fig. 2.8.

Maya-chart is used for the track data. The irregularity of alignment is not a real, value, but a middle point deviation value from measuring standard line which is a 10 m chord as expressed in Fig. 2.9. In the simulation, however, a real wave form has to be provided, and so it is necessary to produce original wave form by any possible means.

Detail technique of this production is described in Appendix III.

The procedure to make the track data for simulation from Maya-chart is as follows:

- (1) Trace the wave form of Maya-chart on recording paper with black ink for curve reader, because of the difficulties to read directly from Maya-chart with the present curve reader. To improve this, the records of Maya-chart have to be recorded on magnetic tape in parallel, and then the tape may be available for computation directly.

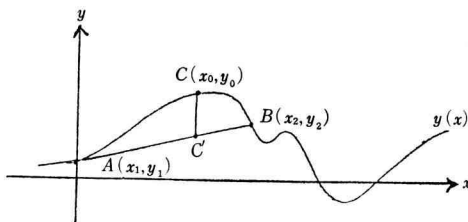


Fig. 2.7 Algorithm to transform a wave form into a folded line

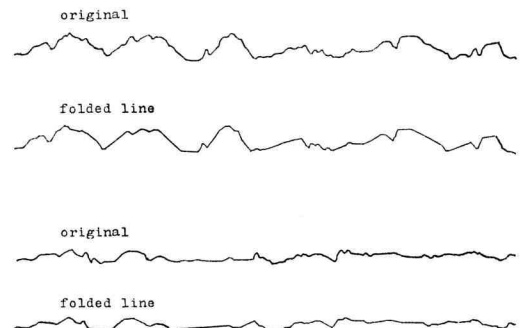


Fig. 2.8 Folded lines transformed from measured wave forms of track

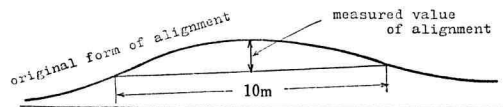


Fig. 2.9 Measurement of alignment irregularity

- (2) Read the wave form with curve reader, and make a data tape. It is sufficient to express about 450 points for 300 m section.
- (3) The cord of tape is transformed so as to fit the computer cord, if necessary. For instance, 8 bit mode curve reader tape is changed to 7 bit mode one for the computer.
- (4) Simplify the input data of wave form to a folded line and make a data tape. The data of alignment are transformed by Fourier series to reproduce the original wave form.

2.4 Representation including curved track sections

In case of a car passing a curved track, the simulation program for straight track is available with some modification. It is a general one which contains transition parts of entrance and ending of curves.

External forces produced in accordance with passing curved track are centrifugal force and yawing moment, and the simulation for curved track can be developed by adding these forces to standard program.

Centrifugal acceleration on a curved track is:

$$\alpha = -v^2/R \quad (2.28)$$

where v is advancing speed and R is radius of curvature, positive for turning left.

The angle of cross level of track by cant is represented by θ . The effective centrifugal acceleration α_{eff} is,

$$\alpha_{\text{eff}} = \alpha \cos \theta - g \sin \theta \quad (2.29)$$

Centrifugal forces are taken to a kind of track data, and stored in digital computer memories in form of a folded line as in Fig. 2.10. The data at every moment is given to analogue part after changing a digital value through DA converter, where $\beta/10\omega_3$ in the figure is a scale factor to match analogue program.

The car body centrifugal acceleration is shown as,

$$\alpha = (\alpha_1 + \alpha_2)/2 \quad (2.30)$$

where α_1 and α_2 are the accelerations at the front and the rear axle, respectively.

A moment in yaw is produced by the car body moment of inertia at the entrance or the exit of curved section. So on the car body, the angular acceleration is:

$$m = (\alpha_1 - \alpha_2)/(2a) \quad (2.31)$$

(To input analogue part, scale factor is $\alpha\beta/(10\omega_4)$. This moment is sent to DA 7 in Fig. A1.3.)

To compensate a centrifugal force, what is called cant is provided in a curved section. The difference of cant at the front axle and the rear axle twists car body. The effect of twisting is represented by modifying cross level of track. In case difference of cant between the location of front axle and rear axle is Δk , $-\Delta k/4b$ is added to the cross level at front axle, and is subtracted at rear axle. (Cross levels input are DA4, DA5 in Fig. A1.4.)

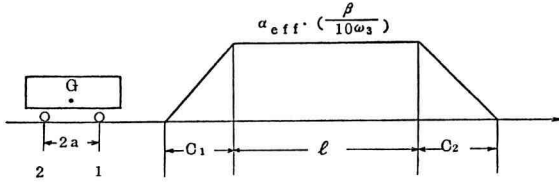


Fig. 2.10 Centrifugal force

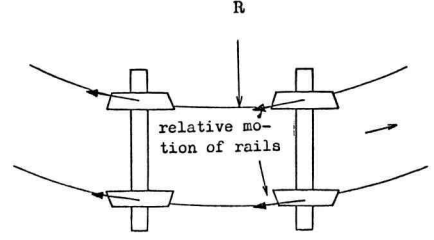


Fig. 2.11 Relative motion between wheelsets and rails in curved track

Relative advancing speed of left and right wheels against each rail are different on running a curved track. Therefore a modification is necessary to the formulas of creep force, that is, for front wheelset,

$$Q_{1L}^{\circ} = f_1(b\dot{\psi}/v + \Delta r_L/r + \Delta v/v) \quad (2.32)$$

$$Q_{1R}^{\circ} = -f_1(b\dot{\psi}/v - \Delta r_R/r + \Delta v/v) \quad (2.33)$$

where

$$\Delta v/v = b/R \quad (2.34)$$

It is similar for rear wheelset. Relative movement between rail and wheelsets differs in front and in rear as shown in Fig. 2.11. The creep forces in lateral direction, therefore, differ also with those wheelsets, that is, for front wheelset,

$$Q_{2L1}^{\circ} = -f_2\{\dot{y}_1/v - (\psi_1 - \bar{\psi}_R)\}/\cos \alpha_L \quad (2.35)$$

$$Q_{2R1}^{\circ} = -f_2\{\dot{y}_1/v - (\psi_1 - \bar{\psi}_R)\}/\cos \alpha_R \quad (2.36)$$

for rear wheelset,

$$Q_{2L2}^{\circ} = -f_2\{\dot{y}_2/v - (\psi_2 + \bar{\psi}_R)\}/\cos \alpha_L \quad (2.37)$$

$$Q_{2R2}^{\circ} = -f_2\{\dot{y}_2/v - (\psi_2 + \bar{\psi}_R)\}/\cos \alpha_R \quad (2.38)$$

where

$$\bar{\psi}_R = a/R$$

At the entrance and the exit of curved track, similarly to the centrifugal force, a mean value of front and rear wheelset is used as $\bar{\psi}_R$.

The input data for the simulation program are,

- N : number of curved track sections
- L_1 : beginning point of each curve
- L_2 : ending point of each curve
- T_1 : length of transition curve at the entrance
- T_2 : length of transition curve at the exit
- R : radius of curvature, positive to turn left
- K : cant, positive to right side high

For a track shown in Fig. 2.12, for example, $N=2$, and on the first curve, $L_1=0(m)$,

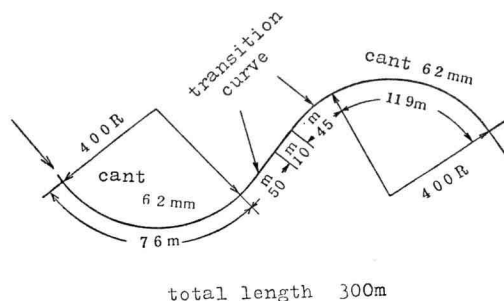


Fig. 2.12 An example of a curved track

$L_2=76$, $T_1=0$, $T_2=50$, $R=400$, $K=0.062$ (m), and on the second curve, $L_1=181$ (m), $L_2=300$, $T_1=45$, $T_2=0$, $R=-400$ and $K=-0.062$ (m).

3. Running Experiment of Railway Cars

Various kinds of running test were commonly carried out in parallel to theoretical survey to obtain vibrational characteristics or to check running safety of railway cars. For these tests, however, service lines were used and so the tests were limited within a safe range. Accordingly it was impossible to grasp the process of derailment. Thus, to study derailment phenomenon, a test line had been constructed to run test cars with no man on it. Measured data were sent to measurement station on FM telemeter. The observation of derailment process was carried out, which had been impossible on service line tests, and the experiments by changing severely the conditions of track, car, car load or car speed could be performed.

3.1 Summary

An outline of the test is as follows:

a. Objective for test line installation

- (1) Clarification of derailment phenomenon with an actual car
- (2) Survey on the effects of track and car conditions on derailment
- (3) Certification of various countermeasures effect to increase safety for running car
- (4) Certification of the guarding device effect against derailment

b. Installation site of test line

The test line was chosen about 10 kmlong, between NIINAI and SHINTOKU, on the old Nemuro trunk line, Kamikawa, Hokkaido. A plan view and a longitudinal section view are shown in Fig. 3.1.

c. Test period

Tests were carried out from 1967 to 1971.

d. Testing method

- (1) A test train is composed of two cars, that is, a test car and an instrument car which is equipped with tele-meter oscillator, video recorder, etc. It is pulled up by a

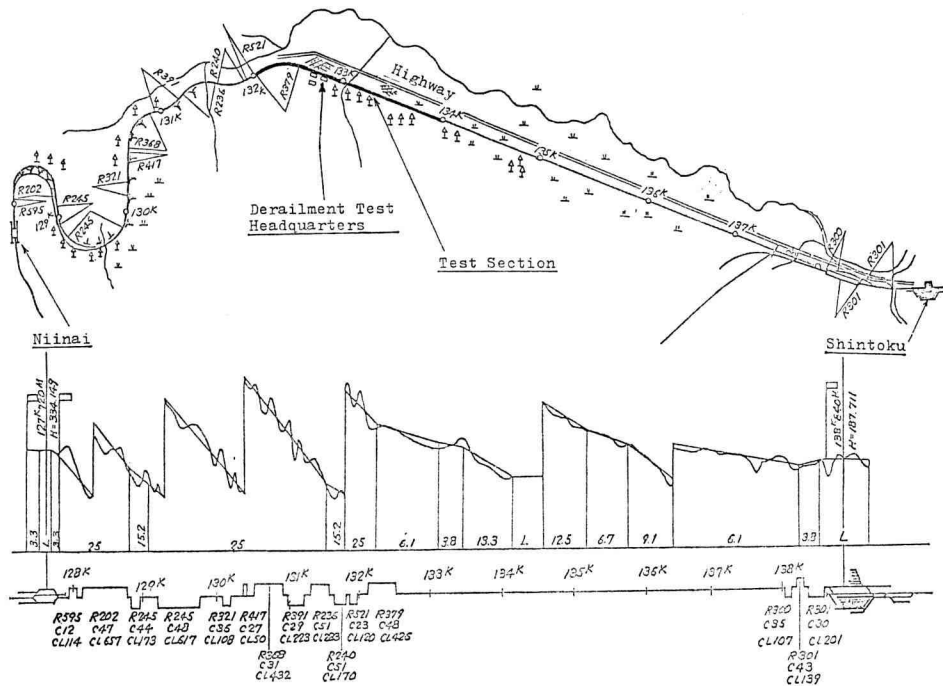


Fig. 3.1 Derailment Test Line

locomotive, and is released at a planned point to make itself accelerate due to down grade.

- (2) Deceleration and stop control of the test train after releasing is done at the instrument car by receiving tele-control (remote control by telemeter) from the ground.
- (3) Measured data are sent to the ground on FM telemeter wave and recorded.
- (4) No man is on the test train in test running. The outline is shown in Fig. 3.2.

e. Conditions of tests

(1) Test car

Using 2-axle freight cars, the degree of eccentric loading in the lateral direction, difference of diagonal wheel loads sums, difference of right and left wheel radius, parallelness of front and rear axle, spring constant of bearing spring, frictional coefficient of bearing spring, side clearance of journal bearing, etc., are varied, and compared with those under standard conditions.

Using bogie freight cars, the degree of overloading, difference of right and left wheel radius, clearance of side bearers, spring constant of bolster spring, frictional coefficient of bolster spring, etc., are varied, and their effect upon derailment are investigated.

(2) Track

As the conditions of tracks, both in a curved section with radius of 400 m and in a straight section, irregularities in alignment and in cross level with sinusoidal wave

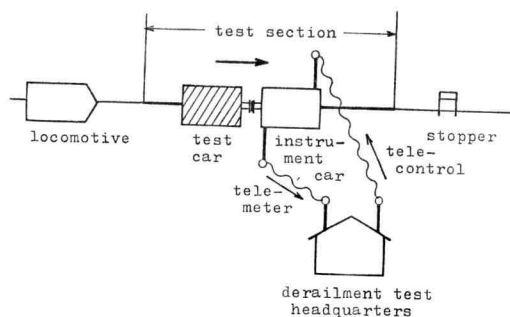


Fig. 3.2 Outline of testing method

form of three cycles are given. The waves are varied in their height and length. Alignment and cross level are in inverse phase, that is, when alignment deviates to the right, cross level is set as right side low.

f. Main items of measurement

(1) Car

Side thrust of wheels, wheel load, vibrational acceleration of car body, deflection of bearing springs, relative displacement between axle box and car body, and behavior of wheels with a video recorder camera

(2) Track

Lateral displacement of rails

3.2 Method of experiment

A locomotive and a test train composed of a test car and an instrument car in order are pulled up to releasing point, which is fixed for the test train to pass the test section at planned speed after releasing from the locomotive.

At the releasing point, preparations are done, such as starting the video recorder, blowing a siren fixed to the instrument car, and then all members get off the test train. On receiving an order from the head quarter, the locomotive pulls the train up just a bit and at that moment a coupler between the locomotive and the test train is opened, and the test train runs freely on a down grade track.

System of measurements and speed control of the test train are explained in Fig. 3.3. Test car informations, such as vibrational acceleration of car body, various parts relative displacement, wheel side thrust, wheel load are transduced to electric signals and transferred to instrument car through the electric connecting plug. The signals are amplified, modulated, and sent with telemeter.

On the other hand, receiving apparatus is set in a used bus on the ground, called an adjustment car, and there they receives waves of telemeter through the specially installed antenna, reproduces and records on oscillographs.

The test train is decelerated and stopped by tele-ontrol after passing through the test sections. The locomotive is called back to be coupled to the test train after being

confirmed no mistake and ending the track measurements. Then follows the next test running.

When derailment appears in the test run, a derailment detector of the test car works, and a coupler between the test car and the instrument car is automatically opened, and the electric connection is also opened, and so the instrument car and its contents are made

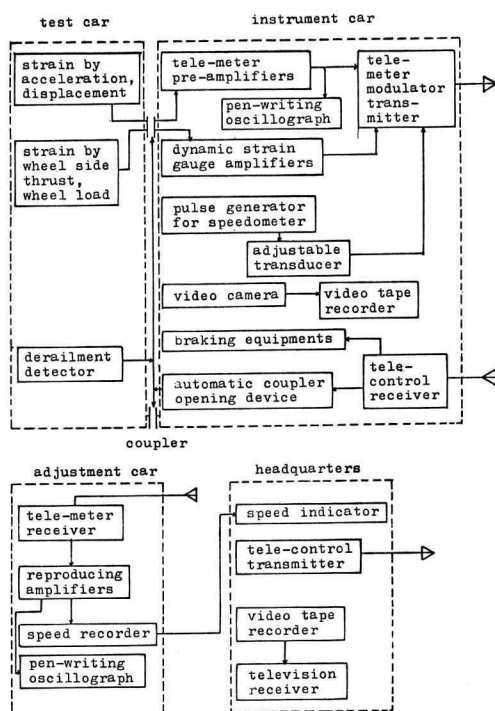


Fig. 3.3 System of measurement

free from damage. The instrument car itself is made its center of gravity lower by placing dead load on the floor, its wheel flanges higher, and the flange angle wider by 10° . The above measures make the instrument car safer against derailment at the sacrifice of heavy body weight and of wheel wear increase.

Major items of measurement and their method are mentioned in the following items:

(1) Wheel load, wheel side thrust

Strains of wheel spokes are measured to get wheel load and wheel side thrust. Strain gauges are attached to the spokes, and are set up bridge circuits as in Fig. 3.4. Lead wires are connected to dynamical strain amplifiers through slip rings.

Wheelsets with spokes at the wheels are chosen for measurement. Holes for lead wires and for screws are drilled to the axle as shown in Fig. 3.5. Wire strain gauge are used for stress measurement. Considering temperature variation and stress magnitude,

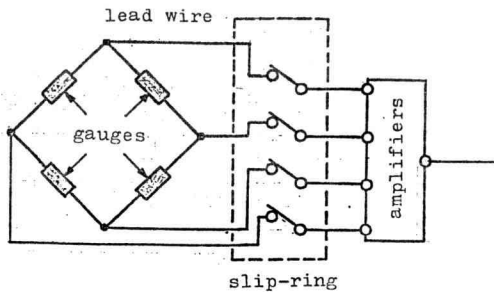


Fig. 3.4 Bridge circuit for measuring wheel forces

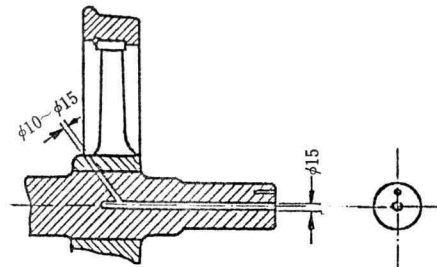


Fig. 3.5 Hole at axle end for lead wires

Polyester 120 Ω resistance gauges with 10 mm \times 3 mm size and 27 mm \times 8 mm base are used.

Adhesive for the gauges is polyester type by mixing two kinds of liquid available under normal temperature. The attached gauges are protected from moisture. There are two ways for this treatment, permanent one and temporary one. The latter is easy for mending, and fits in this case. Coating is done with yellow wax with melting point of 50°C.

The gauges attached on spokes of wheel are connected as bridges, which are different for wheel side thrust measurements and for wheel load ones. The output wave form of wheel side thrust is continuous and that of wheel load changes its sign for each half revolution.

Attached gauges positions and connection networks are shown in Fig. 3.6. The connected two sets of lead wires for wheel load and for wheel side thrust are pulled out through the hole at journal end, and are soldered to slip ring terminals.

Calibration is carried out by applying actual forces to the wheel: Pushing out right and left wheels with pressure of 0 to 3tf or 0 to 5tf for wheel thrust, and running the car at very low speed along the straight and plane track for wheel load. The connection of wire strain gauges to measure wheel side thrust is as to pick up bending stress of wheel spokes and to make the affection of wheel load and of temperature variation negligible, and that to measure wheel load is to form rectangular wave with sign change for each half cycle. On the calibration little and negligible deviation on sensitivity has to be confirmed by varying the forcing point position to the wheel.

The length of a pin attached at the wheelset axle end to drive slip rings is determined under considering relative movement of axle and axle box. Pin material is chosen not to be broken in running, soft but wear allowable. Slip rings must be stable, small electric resistance and strong against wear. Its general view is shown in Fig. 3.7.

(2) Vibrational acceleration and displacement

Transducers applying wire strain gauge are used for measuring car body vibrational acceleration. Their principle is, as in Fig. 3.8, to take out the strain of leaf spring suspending a weight.

Displacement is also transduced to strain of a spring as in Fig. 3.9.

(3) Detection of derailment, electric connector

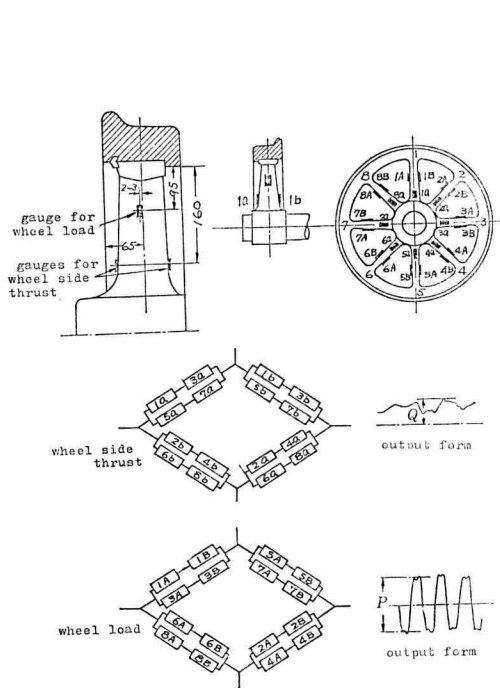
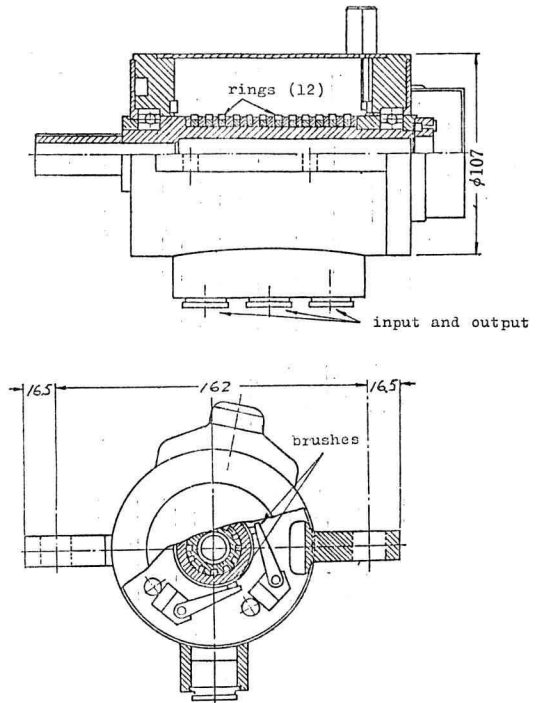
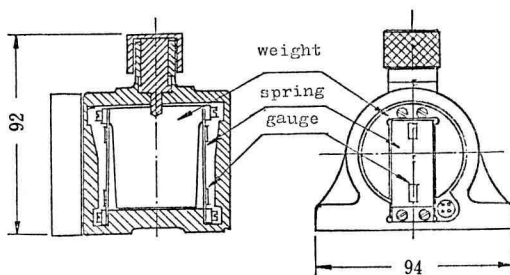


Fig. 3.6 Attached positions of gauges and their connections



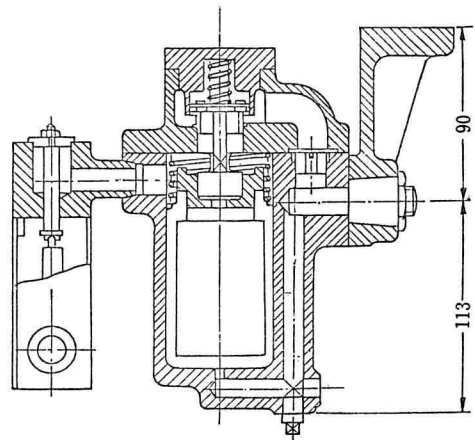
brush material: silver graphite alloy
ring material: silver base copper-cadmium alloys
weight: 4.2 kgf max. speed: 17000 rpm

Fig. 3.7 Slip-rings



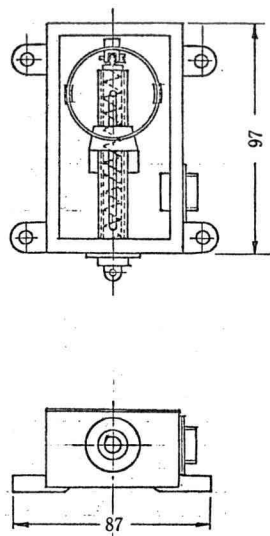
measurement direction: horizontal
measurement range : 1 g
natural frequency : 12 Hz
output for 1 g : 3200×10^{-6}
strain gauge : $120\Omega \times 4$ (bakelite)
damping : air damper

Fig. 3.8 Vibrational acceleration transducer (horizontal)



work at 3 g or over of vertical acceleration

Fig. 3.10 Derailment detector



measurement range: 60 mm
 spring tension : 1~4 kgf
 output : $\pm 2000 \sim 2500 \times 10^{-6}$

Fig. 3.9 Displacement transducer (strain gauge type)

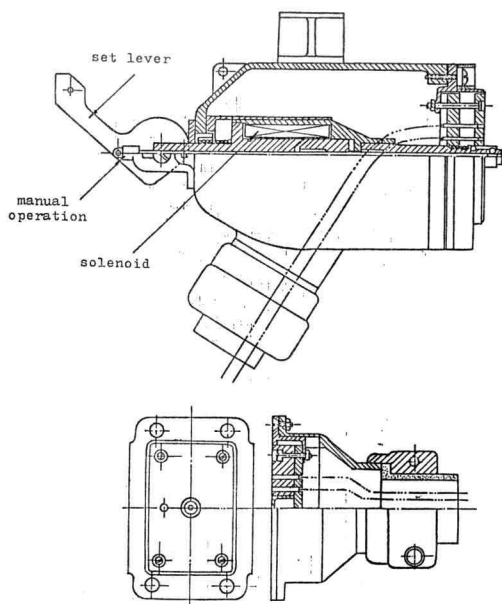


Fig. 3.11 Electrical circuit connector (100 lines)

In case that the test car, which is coupled behind the instrument car, derails or overturns, the instrument car is pulled backwards and becomes dangerous by breaking of coupler or by derailing the test car. To prevent the danger, a derailment detector is attached to the test car, and on derailment the device acts to open both the coupler and connector of electrical circuits between the test car and the instrument car.

Derailment detector and electrical circuits connector are shown in Fig. 3.10 and Fig. 3.11, respectively.

(4) Test car speed

The speed is measured from axle revolution number of the instrument car, which is the same as a test car when they are in coupling.

(5) Relative position of wheel and rail, and others

To record relative position of wheel against rail, a mechanical way or using movie may be considered, but here they are recorded on video tape recorder with an industrial television camera. The motion of wheel can be reproduced just after each test, and thus the condition of the following test can be settled promptly.

Car position in running is picked up from the ground to the instrument car with an electrical magnetic way.

The electric power for measurements is generated with a diesel electric generator, AC 100 V, 50Hz.

3.3 Results of experiment

An example of records of wheel load and wheel side thrust is shown in Fig. 3.12. When the test car is passing through the beginning point of the first wave of track irregularities, the load of left wheel of a front wheelset decreases to an extreme value $1'$ because the first wave of track irregularities begins from the left side for train running direction. With further advancing of the car, the wheel side thrust of the same side increases by two extreme values, Q_1 , Q_2 , or one value in some cases, and then decreases. After that the wheel load and the wheel side thrust of the right wheel vary in a same manner and their extreme values are obtained. This manner is a fairly standard variation for this wave form track irregularities. The variation continues by 7 after passing the end of the track irregularities.

The wheel load diminuation is related with track irregularities in alignment and in cross level, and also with inertia force of car body. The wheel side thrust increases rapidly to an extreme value just after the contact of wheel flange and rail, whereas it is very small in value during the tread of wheel moving laterally on a rail without wheel flange and rail contract. The wheel side thrust becomes no progress by the time when clearance between wheel axle and car body are closed, and after that it increases again to the second extreme value by the lateral motion of wheelset pushed by car body inertia. Then the wheelset and the car body move to the opposit side, and the similar variation of wheel side thrust occurs at the opposit side wheel.

Data processing is carried out as the following way: Read the extreme values of wheel side thrust for each wave of track irregularities. For left wheel, one more value is

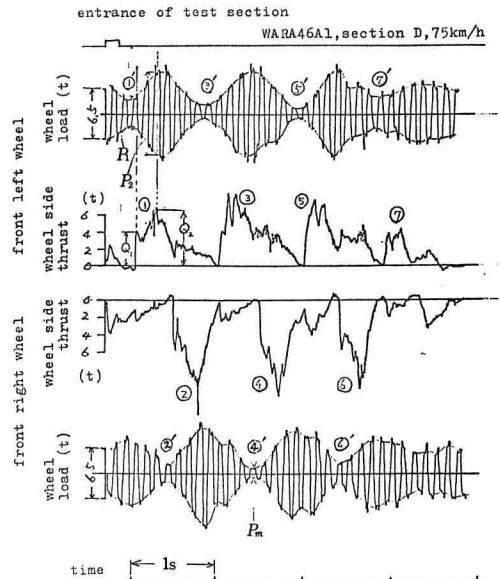


Fig. 3.12 Wave forms of wheel load and wheel side thrust

read just after passing the test section. The values with frequency higher than 50Hz are cut off. Accordingly, 8 values for the left wheel and 6 for the right wheel are obtained in one test section. The values of wheel load at the points, where above-mentioned wheel side thrusts are produced, are read, and the ratios of wheel side thrust to wheel load, (Q/P) , are calculated. The extreme values of wheel load reduction, produced to right and left wheel alternatively, are read and the rates of wheel load reduction, $(\Delta P/P_s)$, are obtained, where P_s denotes static wheel load and ΔP does the value of wheel load reduction.

The maximum values of Q , Q/P and $\Delta P/P_s$ for one test track section are denoted "the maximum values for the test section", and the values are plotted against car speed.

As the wheel side thrust for the inner side of track on curved test section is far smaller than that for outer one, data are picked up only from the outer side one, that is, left wheel in this test, except for special problems. On straight test section, the data are picked up from both sides of wheelset, and the maximum values are plotted in a figure. In case wheel-climbing-up on rail occurs, the maximum value just before wheel-climbing-up is plotted.

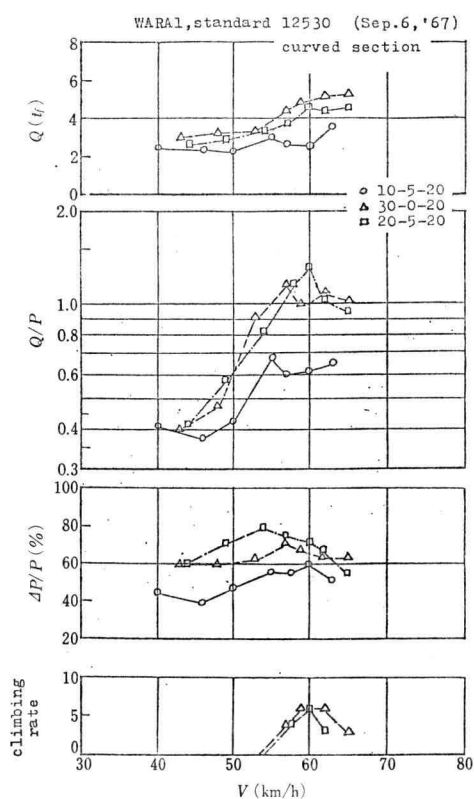


Fig. 3.13 Characteristics values in curved test section

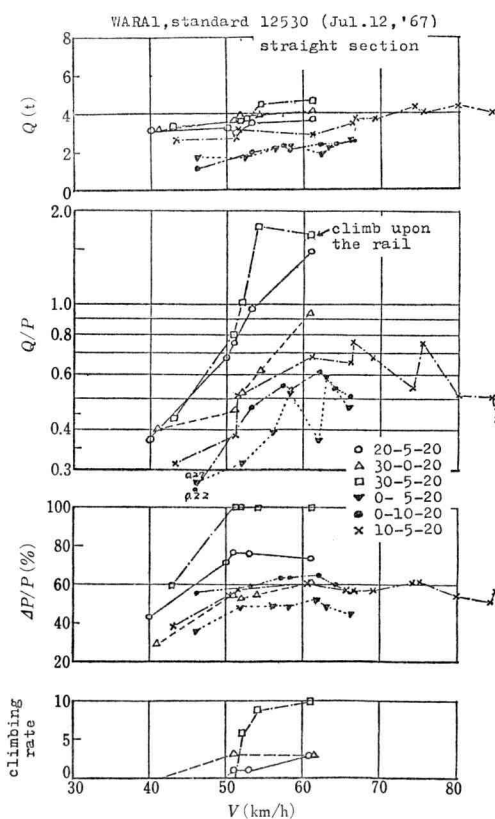


Fig. 3.14 Characteristic values in straight test section

On the derailment on service lines in the past and on these tests which include the case that a wheel flange climbs on rail, there has been almost no case that the rear wheel derailed first, and so it is almost true that the derailment, without any definite cause such as breaking out of some parts of car or rail, would happen at the front wheelset. The running safety is, therefore, checked on a front wheelset except a special problem exists.

When a wheel is climbing rail, the motion of the wheel relative to rail is recorded on magnetic tape with an industrial television camera which is set under the body of instrument car. A point system is applied when clearance is seen between the wheel tread and the rail surface. The clearance can be observed from reproducing scene of video recorders. Climbing point 1 is given for the clearance between wheel tread and rail less than 3 mm, and climbing point 3 is given for the clearance over 3 mm except the wheel flange is entirely climbing up rail, which is climbing point 10. The sum of the points for each of right and left wheel during a test section is denoted "climbing rate" of the wheel. In the figure the larger one from the two of the right and the left is shown. In the tests, the derailment prevention guards are equipped and so in case a wheel flange climbs upon a rail, which occurs many times, the wheel is brought back and so actual derailment occurs only few times. The climbing rate of 10 in general service line is considered to connect directly with derailment.

Figure 3.13 and Fig. 3.14 show the characteristic values for curved and straight track section. The derailment occurs in the straight section of (30-5-20) at the running speed of 61 km/h. Against various car conditions, these figures are obtained and the effects of the conditions on derailment have been clarified.

4. Evaluation of the Simulation

Suppose a general name "Derailment simulator" is given to a program of simulation, combined with its machines and equipments. The simulator of prototypo is produced at first and then improved to practical use.

4.1 General of the derailment simulator

On putting a stress point to derailment, wheel load and wheel side thrust are suitable as the outputs of the simulator. Figure 4.1 shows the process of making the simulator. A hybrid computer is used in this report. The model of a car is settled. The simulation program is made based on the theoretical analysis and also on the phenomena observed in the test line experiments. Data of the experiments of actual car and of the test, which is carried out to survey a derailment accident, are collected for the simulator. Repeating the simulation process and improving the accuracy, the simulator is developed and improved.

Figure 4.2 is a comparison of running test wave form with simulator outputs. Coincidence of timing and of wave height are seen from the figure.

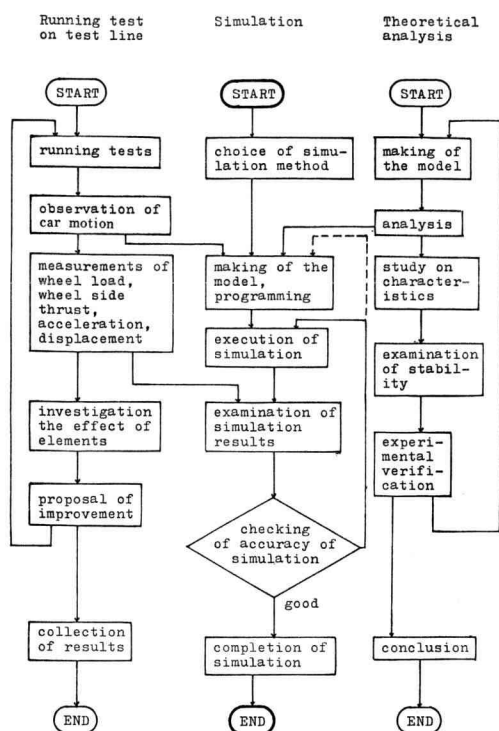


Fig. 4.1 Manufacture of simulator

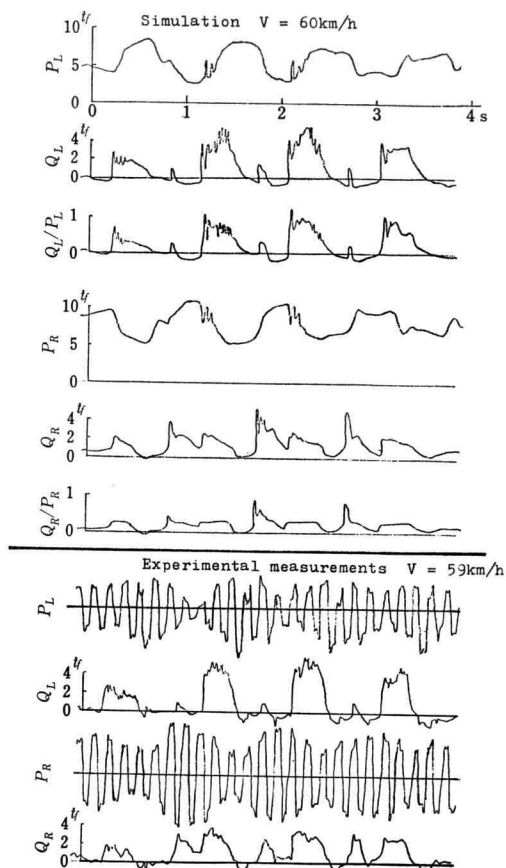


Fig. 4.2 Comparison of the results of simulation and experiment

4.2 Effectiveness of the simulator

The application examples of simulator are explained as flow charts in Fig. 4.3. The simulator is first applied to survey the causes of a derailment accident, and an example is shown in Fig. 4.4. The upper waves in the figure are track data measured with track inspection car, and the lower waves are the outputs of simulator. The derailment is guessed to be occurred that the front right wheel side thrust is produced at the time when the wheel load is extremely diminished, and at that moment the wheel flange contacts the rail and then the wheel begins to climb upon it.

The next application of the simulator is the additional survey on the effects of the factors and of their combinations with derailment. Because the running tests must be carried out under many severe conditions and restrictions such as test car operation or track adjustment, in other words, the running tests are very hard for us to carry out.

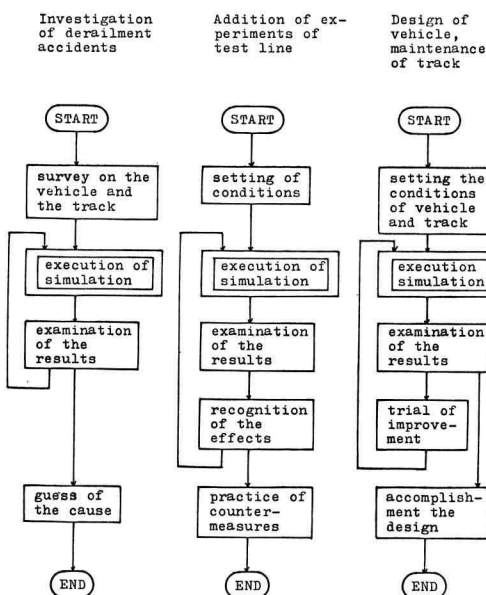


Fig. 4.3 Application of simulator

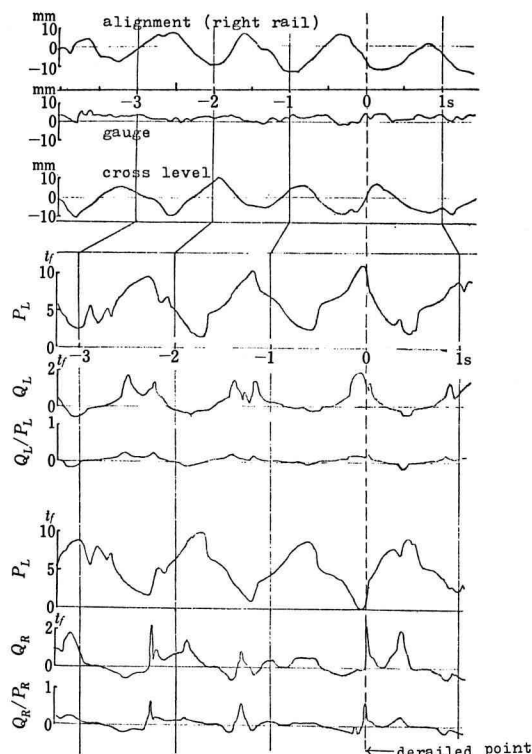


Fig. 4.4 An example of the simulation for a derailment accident

5. Concluding Remarks

On the behavior of railway cars in running, study was carried out with special attention to derailment relations. The body motions of a railway car have six degrees-of-freedom, that is, longitudinal, lateral, vertical, yawing, rolling and pitching motions. Among them the lateral, yawing and rolling motions were studied in this report, because of their deep connection with derailment. The vertical and pitching motions are supposed to be secondary for the effect on derailment as can be seen in running tests and they are separable from the lateral one.

A wheelset of railway car has a character of producing self-excited vibration in the lateral direction, the cause of which are the conicity of wheel tread and rigid connection of right and left wheels. One of the problems on the car stability in the lateral motion, therefore, is to suppress the wheelset instability.

To study on derailment, theoretical model is taken as similar an actual car as possible, and so it becomes complicated with many non-linearities. Hybrid computer, which consists of the combination of analogue computer and digital computer, is assumed to be effective and the simulator has been developed with the computer. Dimensions of car, clearances, friction, etc., are set in the analogue part of the hybrid computer, and track data

and a part of car data are stored and taken out from the memories of the digital part. Some of the calculation of non-linearities are also under the charge of the digital part.

Forces acting between wheel and rail play an important role in the simulation. The forces acting to a wheel are calculated with relation to a wheel tread profile, a rail profile and the slight relative speed produced between the wheel and the rail. Track irregularities are stored in distance base in memories of the digital part as the wave forms of alignment, cross level and gauge width which have been measured in advance. Each wave form is considered to represent a folded line, and in making the folded line, it is especially conceived that the peak values of the wave are unchanged and the deviation from the original wave is limited within a given quantity. To accomplish the simulation, data of actual running tests on a test track are used.

The running tests were carried out on the test track at Karikachi, Hokkaido. An instrument car, loaded up measuring instruments, and a test car were coupled and rushed along down grade track with no man inside, and the measured data were transmitted through FM telemeter.

Thus the simulator has been developed and contributes much to apply to the survey of actual derailment accidents and to give the informations for presumption of their causes.

Targets of future progress are considered to broaden its application extent to the fields of design and maintenance, to develop a simulator on bogie railway car, and to add the effects of other cars in a train through coupling devices.

Appendix I Analogue Computation Details

Scaling is necessary for programming of analogue computation. Substituting $\xi = a\beta$, $\zeta = h\phi$, and multiplied by β in length, by 10 in time, the equations from (2.1) to (2.7) are transformed as follows:

$$(10\beta/\omega_1) \ddot{y}_1 = -(\omega_1/10)x_1 - \omega_1\tau_2\dot{x}_1 - (\omega_1/10)f_{y1}(x_1) + \beta/(10\omega_1m_w) \cdot (Q_{R1} + Q_{L1}) \quad (A1.1)$$

$$(10\beta/\omega_2) \ddot{\xi}_1 = -(\omega_2/10)s_1 - \omega_2\tau_1\dot{s}_1 + ab\beta/(10\omega_2m_wi_w^2) \cdot (Q_{1R1} - Q_{1L1}) \quad (A1.2)$$

$$(10\beta/\omega_1) \ddot{y}_2 = -(\omega_1/10)x_2 - \omega_1\tau_2\dot{x}_2 - (\omega_1/10)f_{y2}(x_2) + \beta/(10\omega_1m_w) \cdot (Q_{R2} + Q_{L2}) \quad (A1.3)$$

$$(10\beta/\omega_2) \ddot{\xi}_2 = -(\omega_2/10)s_2 - \omega_2\tau_1\dot{s}_2 + ab\beta/(10\omega_2m_wi_w^2) \cdot (Q_{1R2} - Q_{1L2}) \quad (A1.4)$$

$$(10\beta/\omega_3) \ddot{y}_B = (\omega_3/20)(x_1 + x_2) + (\omega_3/2)\tau_2(\dot{x}_1 + \dot{x}_2) + (\omega_3/20)\{f_{y1}(x_1) + f_{y2}(x_2)\} \quad (A1.5)$$

$$(10\beta/\omega_4) \ddot{\xi}_B = (\omega_6^2/20\omega_4)(x_1 - x_2) + (\omega_6^2/2\omega_4)\tau_2(\dot{x}_1 - \dot{x}_2) + \omega_6^2/20\omega_4\{f_{y1}(x_1) - f_{y2}(x_2)\} + (\omega_6^2/20\omega_4)(s_1 + s_2) + (\omega_6^2/2\omega_4)\tau_1(\dot{s}_1 + \dot{s}_2) \quad (A1.6)$$

$$(10\beta/\omega_7) \ddot{\xi}_B = (\omega_8^2/20\omega_7)(x_1 + x_2) + (\omega_8^2/2\omega_7)\tau_2(\dot{x}_1 + \dot{x}_2) + (\omega_8^2/20\omega_7)\{f_{y1}(x_1) + f_{y2}(x_2)\} + (\omega_9^2/20\omega_7)(p_1 + p_2) + (\omega_9^2/2\omega_7)\tau_3(\dot{p}_1 + \dot{p}_2) + (\omega_9^2/20\omega_7)\{f_{x1}(p_1) + f_{x2}(p_2)\} - (gh/10\omega_7i_x^2)R \quad (A1.7)$$

where,

$$\begin{aligned} \omega_1 &= \sqrt{k_y/m_w}, & \omega_2 &= \sqrt{k_x b_1^2/m_w i_w^2} \\ \omega_3 &= \sqrt{k_y/m_B}, & \omega_4 &= \sqrt{(a^2 k_y/m_B i_x^2) + (b_1^2 k_x/m_B i_x^2)} \\ \omega_5 &= \sqrt{k_x b_1^2/m_B i_x^2}, & \omega_6 &= \sqrt{a^2 k_y/m_B i_x^2} \\ \omega_7 &= \sqrt{(h^2 k_y/m_B i_x^2) + (b_1^2 k_x/m_B i_x^2)} \\ \omega_8 &= \sqrt{h^2 k_y/m_B i_x^2}, & \omega_9 &= \sqrt{b_1^2 k_x/m_B i_x^2} \\ \tau_1 &= c_x/k_x, & \tau_2 &= c_y/k_y, & \tau_3 &= c_x/k_x \\ x_1 &= \beta X_1, & x_2 &= \beta X_2, & s_1 &= \beta a S_1, & s_2 &= \beta a S_2 \\ p_1 &= \beta h P_1, & p_2 &= \beta h P_2, & R &= \beta y_B - (\beta y_1 + \beta y_2)/2 \end{aligned}$$

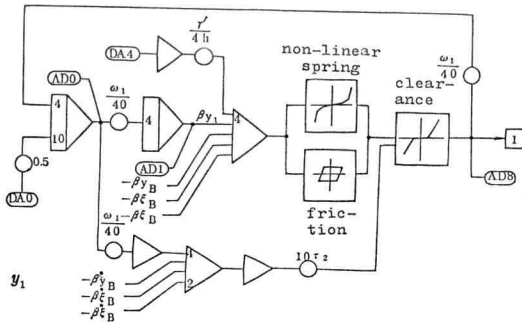


Fig. A1.1 Block diagram for front wheelset

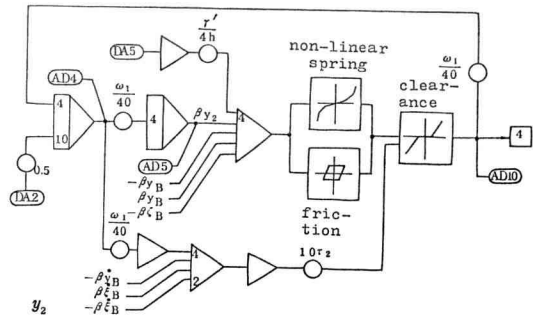


Fig. A1.2 Block diagrams for rear wheelset

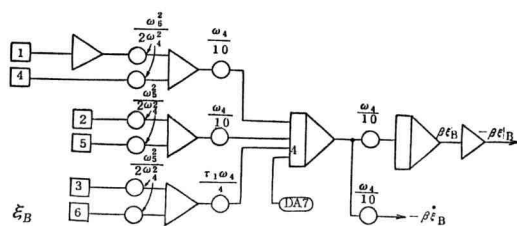
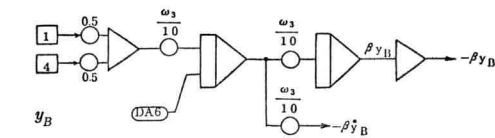
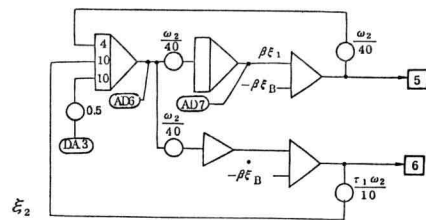
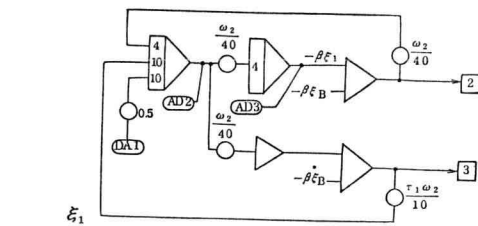


Fig. A1.3 Block diagrams for body lateral and yawing motion

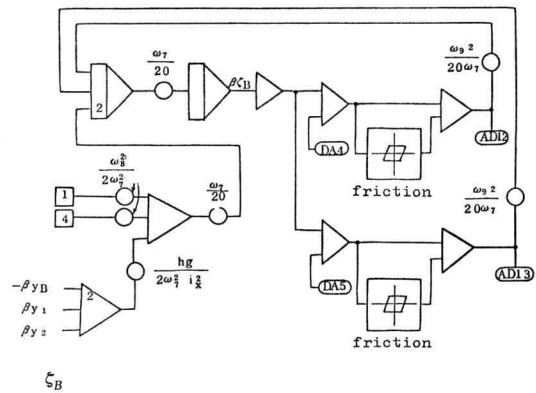


Fig. A1.4 Block diagram for body rolling

$$\begin{aligned} f_{y1}(x_1) &= F_{y1}(X_1)/k_y, & f_{y2}(x_2) &= F_{y2}(X_2)/k_y \\ f_{z1}(p_1) &= F_{z1}(P_1)/k_z, & f_{z2}(p_2) &= F_{z2}(P_2)/k_z \end{aligned}$$

The new unit of time is used for differentiation.

The analogue computer program for 2-axle car is shown from Fig. A1.1 to Fig. A1.4, which contain non-linear restoring force by double link suspension gear and by clearance between axle box and pedestal, and clearance at journal part.

Appendix II Hybrid Computation Details

The following variables are connected to AD converters in the analogue program shown from Fig. A1.1 to Fig. A1.4.

$$\text{AD } 0 \dots y_1^0 \quad (\text{A2.1})$$

$$\text{AD } 1 \dots \bar{y}_1 \quad (\text{A2.2})$$

$$\text{AD } 2 \dots \xi_1^0 \quad (\text{A2.3})$$

$$\text{AD } 3 \dots \bar{\xi}_1 \quad (\text{A2.4})$$

$$\text{AD } 4 \dots y_2^0 \quad (\text{A2.5})$$

$$\text{AD } 5 \dots \bar{y}_2 \quad (\text{A2.6})$$

$$\text{AD } 6 \dots \xi_2^0 \quad (\text{A2.7})$$

$$\text{AD } 7 \dots \bar{\xi}_2 \quad (\text{A2.8})$$

$$\text{AD } 8 \dots Y_1 \quad (\text{A2.9})$$

$$\text{AD } 10 \dots Y_2 \quad (\text{A2.10})$$

$$\text{AD } 12 \dots Z_1 \quad (\text{A2.11})$$

$$\text{AD } 13 \dots Z_2 \quad (\text{A2.12})$$

Representing real time by t , and computation time by τ ,

$$\tau = 10t \quad (\text{A2.13})$$

Writing $\dot{y}(t)$ as differentiation of y with t , and $\dot{y}(\tau)$ as that with τ , the input variables are transferred as follows:

$$y_1^0 = -(10\beta/\omega_1) \dot{y}_1(\tau) = -(\beta/\omega_1) \dot{y}_1(t) \quad (\text{A2.14})$$

$$\begin{aligned} \xi_1^0 &= -(10\beta/\omega_2) \dot{\xi}_1(\tau) = -(10\beta/\omega_2) a\dot{\psi}_1(\tau) \\ &= -(\beta/\omega_2) a\dot{\psi}_1(t) \end{aligned} \quad (\text{A2.15})$$

$$\bar{y}_1 = \beta y_1 \quad (\text{A2.16})$$

$$\bar{\xi}_1 = \beta \xi_1 = \beta a\dot{\psi}_1 \quad (\text{A2.17})$$

Similar transformations are done for variables with subscript 2 (rear wheelset).

All values under calculation have to be expressed in the range $-1 < x < 1$, because digital calculation is fixed point with absolute value under 1.0.

Denoting

$$M = 50\omega_1 m_w / \beta \quad (\text{A2.18})$$

the creep forces of front wheelset in x direction are, from (2.16), (2.17),

$$Q_{1L}^0/M = (f_1/M)(b\dot{\psi}_1/v + \Delta r_L/r) = K_2(K_1\xi_1^0 + \Delta \bar{r}_L) \quad (\text{A2.19})$$

$$Q_{1R}^0/M = -K_2(K_1\xi_1^0 - \Delta \bar{r}_R) \quad (\text{A2.20})$$

where,

$$K_1 = (20r\omega_0/v\beta) \cdot (b/a) \quad (\text{A2.21})$$

$$K_2 = f_1/20rM \quad (\text{A2.22})$$

$$\Delta\bar{r}_L = 20\Delta r_L \quad (\text{A2.23})$$

$$\Delta\bar{r}_R = 20\Delta r_R \quad (\text{A2.24})$$

It is natural to express these right and left creep forces as a torque, because longitudinal motion of wheelset is not taken into consideration. On the other hand, right and left creep forces are actually different with each other. So to make possible to calculate both cases, the following relations are provided:

$$\Delta\bar{r}_L/20 = (\Delta r_L - \Delta r_R)/2 + \gamma(\Delta r_L + \Delta r_R)/2 \quad (\text{A2.25})$$

$$\Delta\bar{r}_R/20 = -(\Delta r_L - \Delta r_R)/2 + \gamma(\Delta r_L + \Delta r_R)/2 \quad (\text{A2.26})$$

$$0 \leq \gamma \leq 1$$

where $\gamma=0$ represents pure torque and $\gamma=1$ independent forces.

Creep forces in y direction are:

$$\begin{aligned} Q_{2L}^\circ/M &= -(f_2/M)(\dot{y}_1/v - \psi_1)/\cos \alpha_L \\ &= K_4(k_3 y_1^0 + \xi_1)/\cos \alpha_L \end{aligned} \quad (\text{A2.27})$$

$$Q_{2R}^\circ/M = K_4(k_3 y_1^0 + \xi_1)/\cos \alpha_R \quad (\text{A2.28})$$

where,

$$K_3 = -\omega_1 a/v \quad (\text{A2.29})$$

$$K_4 = f_2/a\beta M \quad (\text{A2.30})$$

Value of $\cos \alpha$ is approximately expressed by:

$$(\cos \alpha)/2 = 0.502 - \{(\alpha/2) + 0.06125\} \times 0.41051\alpha \quad (\text{A2.31})$$

Creep force changes gradually to frictional force owing to increasing of creep rate. To obtain wheel load, P_L or P_R , it is necessary for calculating creep and frictional forces. Let P represents the mean of right and left wheel loads, and ΔP increase of left wheel load or decrease of right one, that is,

$$P_L = P + \Delta P \quad (\text{A2.32})$$

$$P_R = P - \Delta P \quad (\text{A2.33})$$

Letting forces $\Delta P'$ and f' are transmitted from car body to wheelset as Fig. A2.1, equilibrium of moment leads:

$$\Delta P'(b_1 + b) + \Delta P'(b_1 - b) = 2b\Delta P + f'r' \quad (\text{A2.34})$$

therefore,

$$\Delta P = (2b_1\Delta P' - f'r')/2b \quad (\text{A2.35})$$

$\Delta P'$ is the sum of spring force and frictional force produced by the rolling of car body, and is equivalent Z_1 or Z_2 of (A2.11) or (A2.12).

By considering scaling of analogue computation,

$$\Delta P_1' = (k_x b_1 / 2\beta h) Z_1 \quad (\text{A2.36})$$

$$f_1' = -(k_y / \beta) Y_1 \quad (\text{A2.37})$$

accordingly,

$$\Delta P_1 / M = K_7 (K_6 Z_1 + Y_1) \quad (\text{A2.38})$$

where,

$$K_6 = k_x b_1^2 / 2h k_y r' \quad (\text{A2.39})$$

$$K_7 = k_y r' / 2b\beta M \quad (\text{A2.40})$$

For the mean wheel load,

$$P = (2m_B + 2m_w) g / 4 \quad (\text{A2.41})$$

$$P_{L1} / M = K_8 + \Delta P_1 / M \quad (\text{A2.42})$$

$$P_{R1} / M = K_8 - \Delta P_1 / M \quad (\text{A2.43})$$

where,

$$K_8 = P / M = (m_B + m_w) g / 2M \quad (\text{A2.44})$$

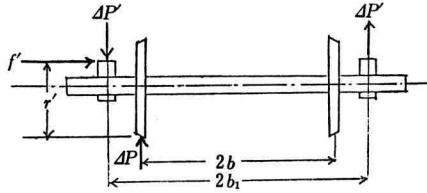


Fig. A2.1 Forces acting to wheelset

On the rear wheelset, calculation can be carried out by changing Z_1 and Y_1 to Z_2 and Y_2 , respectively.

Frictional forces are calculated by (2.19) and (2.20). To obtain the direction of slippage, substitution of θ_L to left wheel leads:

$$|s_{1L}| = |K_{13} \cdot Q_{1L}^\circ / M| \quad (\text{A2.45})$$

$$|s_{2L}| = |K_{14} \cdot Q_{2L}^\circ / M| \quad (\text{A2.46})$$

where,

$$K_{13} = f_2 / (f_1 + f_2) \quad (\text{A2.47})$$

$$K_{14} = f_1 / (f_1 + f_2) \quad (\text{A2.48})$$

and in case $|s_{1L}| > |s_{2L}|$

$$u_1 = |s_{2L}| / |s_{1L}| \quad (\text{A.49})$$

in case $|s_{1L}| = |s_{2L}|$,

$$u_1 = 0.99999 \text{ (maximum value less than 1)} \quad (\text{A2.50})$$

and

$$|\sin \theta_L| = h(u_1) \quad (\text{A2.51})$$

$$|\cos \theta_L| = u_1 \cdot |\sin \theta_L| \quad (\text{A2.52})$$

where,

$$h(u) = 0.49625 / (0.2071u^2 + 0.5) . \quad (\text{A2.53})$$

Similarly, in case $|s_{1L}| < |s_{2L}|$

$$u_2 = |s_{1L}| / |s_{2L}| \quad (\text{A2.54})$$

$$|\cos \theta_L| = h(u_2) \quad (\text{A2.55})$$

$$|\sin \theta_L| = u_2 \cdot |\cos \theta_L| \quad (\text{A2.56})$$

and similarly to the right wheel.

Taking signs as

$$\left. \begin{aligned} \sin \theta_L &= \text{sgn}(Q_{1L}^\circ) |\sin \theta_L| \\ \cos \theta_L &= \text{sgn}(Q_{2L}^\circ) |\cos \theta_L| \end{aligned} \right\} \quad (\text{A2.57})$$

$$\left. \begin{aligned} \sin \theta_R &= \text{sgn}(Q_{1R}^\circ) |\sin \theta_R| \\ \cos \theta_R &= \text{sgn}(Q_{2R}^\circ) |\cos \theta_R| \end{aligned} \right\} \quad (\text{A2.58})$$

Vertical restoring forces are calculated by the expressions (2.21) and (2.22), as follows:

$$N_L/M = P_L/M \cos \alpha_L \quad (\text{A2.59})$$

$$N_R/M = P_R/M \cos \alpha_R \quad (\text{A2.60})$$

Components of frictional force are:

$$F_{\mu L1}/M = \mu N_L/M \sin \theta_L \quad (\text{A2.61})$$

$$F_{\mu L2}/M = \mu N_L/M \cos \theta_L \quad (\text{A2.62})$$

$$F_{\mu R1}/M = \mu N_R/M \sin \theta_R \quad (\text{A2.63})$$

$$F_{\mu R2}/M = \mu N_R/M \cos \theta_R \quad (\text{A2.64})$$

Then creep forces limited by frictional forces are calculated by the expressions (2.23), (2.24), considering that calculation is in fixed point and that no overflow should be appeared.

In case $|F_{\mu L1}| \geq |Q_{1L}^\circ|$

$$Q_{1L}/M = (1/4) \cdot (Q_{1L}^\circ/M) / \{0.25 + (1/4) \cdot |Q_{1L}^\circ/M| / |F_{\mu L1}/M|\} \quad (\text{A2.65})$$

and in case $|F_{\mu L1}| < |Q_{1L}^\circ|$

$$Q_{1L}/M = (1/4) \cdot (F_{\mu L1}/M) / \{0.25 + (1/4) \cdot |F_{\mu L1}/M| / |Q_{1L}^\circ/M|\} \quad (\text{A2.66})$$

(1/4) in the above expressions is to make calculation simple, shifting by 2 bits. Forces of right wheel in y direction can be similarly calculated. Thus, all of Q_{1L}/M , Q_{1R}/M , Q_{2L}/M and Q_{2R}/M are fixed.

Wheel side thrust are obtained from (2.12), (2.14), and as $f_L = Q_{2L}$, $f_R = Q_{2R}$.

$$Q_L/M = -(P_L/M) \tan \alpha_L + (Q_{2L}/M) \cdot (1/\cos \alpha_L) \quad (\text{A2.67})$$

$$Q_R/M = (P_R/M) \tan \alpha_R + (Q_{2R}/M) \cdot (1/\cos \alpha_R) \quad (\text{A2.68})$$

where,

$$\tan \alpha = (\alpha/2) / \{0.5 - (0.77471\alpha - 0.02646) \cdot (\alpha/2)\} \quad (\text{A2.69})$$

The force and the moment to wheelset are calculated by the following expressions, and after DA conversion they are sent to analogue computer.

$$(\text{Force in } y \text{ direction}) = Q_L/M + Q_R/M \longrightarrow \text{DA0, 2} \quad (\text{A2.70})$$

$$(\text{Moment around } z\text{-axis}) = (Q_{1R}/M - Q_{1L}/M) \cdot K_{10} \longrightarrow \text{DA1, 3} \quad (\text{A2.71})$$

where,

$$K_{10} = ab\omega_1/i_w^2\omega_2 \quad (\text{A2.72})$$

Cross level irregularities $\beta_{\xi_1}^{\zeta}, \beta_{\xi_2}^{\zeta}$ are taken out to DA 4, DA 5, respectively.

Wheel load and wheel side thrust are made DA conversion similarly to record on oscillograph paper.

For wheel side thrust,

$$Q_L/M \cdot K_{24}, \quad Q_R/M \cdot K_{24} \quad (\text{A2.73})$$

and for wheel load,

$$P_L/M \cdot K_{16}, \quad P_R/M \cdot K_{16} \quad (\text{A2.74})$$

where,

$$K_{24} = M/8000 \quad (\text{A2.75})$$

which transfers wheel side thrust of 8tf to full scale (40 mm) for a channel of pen-writing oscillograph paper, and

$$K_{16} = M/20000 \quad (\text{A2.76})$$

which makes a full scale equal to wheel load of 20 tf.

One loop of hybrid computation takes 20ms, and the values of wheel tread forces which are obtained by digital calculation are kept constant during the period. It is delayed about 10ms in average. Owing to this delay, in some cases fine vibration is produced. For preventing these phenomena, the values of creep coefficients in (A2.19), (A2.20) or (A2.27), (A2.28) are decreased in small ranges of ξ_1^0, y_1^0 , that is, limited values $c_{m\xi}, c_{my}$ are given to ξ_1^0, y_1^0 , and for $|\xi_1^0| < c_{m\xi}$,

$$K' = K_1 \cdot |\xi_1^0| / c_{m\xi} \quad (\text{A2.77})$$

and for $|\xi_1^0| \geq c_{m\xi}$,

$$K_1' = K_1 \quad (\text{A2.78})$$

Similarly, for $|y_1^0| < c_{my}$,

$$K_3' = K_3 \cdot |y_1^0| / c_{my} \quad (\text{A2.79})$$

and for $|y_1^0| \geq c_{my}$,

$$K_3' = K_3 \quad (\text{A2.80})$$

K_1' K_3' are used for K_1 , K_3 . The above-mentioned excitation can be prevented, but error of simulation becomes larger for small displacement. The motion produced by large irregularities of track makes displacement of wheelset large, and $|\xi_1^0|$, $|\gamma_1^0|$ are also large at the problematic point under severe force, therefore the above errors' affection can be neglected to the aimed phenomena of the simulation.

Appendix III Detail Technique of Original Wave Form Production

Representing $f(x)$ for the absolute alignment of track, and $F(x)$ for the measured alignment with a base line of chord length $2a$, the following relation holds:

$$F(x) = f(x) - \{f(x+a) + f(x-a)\}/2 \quad (\text{A3.1})$$

Assuming that the original wave form is sinusoidal, that is,

$$f(x) = A \sin qx \quad (\text{A3.2})$$

Substituting this to (A3.1),

$$\begin{aligned} F(x) &= A \sin qx - \{A \sin q(x+a) + A \sin q(x-a)\}/2 \\ &= A(1 - \cos qa) \sin qx \end{aligned} \quad (\text{A3.3})$$

which means an original of (A3.2) is transformed to (A3.3). Sinusoidal wave keeps its wave length and phase, and changes only its amplitude by above-mentioned measurement.

Denoting the ratio of measured wave amplitude to original one as s , that is called sensitivity, then,

$$s = A(1 - \cos qa)/A = 1 - \cos qa \quad (\text{A3.4})$$

The relation of wave length and sensitivity is as Fig. A3.1, which shows sensitivities at wave lengths $a, a/2, a/3, \dots$ are zero. A transformation (A3.1) is a linear one, and so the superposition holds, that is, if f_i is transformed to F_i , and

$$f(x) = f_1(x) + f_2(x) + \dots + f_n(x) \quad (\text{A3.5})$$

then,

$$F(x) = F_1(x) + F_2(x) + \dots + F_n(x) \quad (\text{A3.6})$$

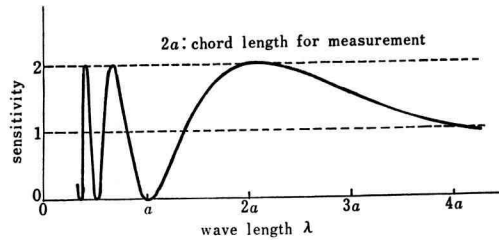


Fig. A3.1 Sensitivity of alignment measurement to wave length

A wave form is generally expanded by a Fourier series. By the relations (A3.5) and (A3.6), the measured wave form can be produced by multiplying sensitivities (A3.4) by each term of the Fourier series for the original wave form and then summing up. The measured wave form does not contain the components with wave length $a, a/2, a/3, \dots$, as their sensitivities are zero. So in principle, the reproduction of original wave form is impossible from the measured one, for lack of informations on above components. Components of wave length from 10 to 30 m, however, are actually important, and so it is

necessary in practical point of view to try to reproduce the original wave form. After a wave form of alignment of track being expanded in Fourier series, the reproducing wave form can be obtained by summing up the terms which are multiplied by the multipliers provided by the relation of (A3.4).

Suppose a wave form with l m in length is given, and is equally divided into r parts, where r is even, and the measured values are denoted by y_0, y_1, \dots, y_{r-1} . Then the Fourier series are approximately written with these discrete points as follows:

$$y_i = a_0 + a_1 \cos x_i + a_2 \cos 2x_i + \dots + a_{(r/2)} \cos (r/2)x_i \\ + b_1 \sin x_i + b_2 \sin 2x_i + \dots + b_{(r/2-1)} \sin (r/2-1)x_i \quad (\text{A3.7})$$

$$x_i = i \cdot 2\pi/r, \quad (i = 0 \sim r-1) \quad (\text{A3.8})$$

where,

$$a_0 = (\lambda_0/r)(y_0 + y_2 + \dots + y_{r-2}) \\ + (\mu_0/r)(y_1 + y_3 + \dots + y_{r-1}) \quad (\text{A3.9})$$

$$a_j = (2\lambda_j/r)(y_0 \cos jx_0 + y_2 \cos jx_2 + \dots + y_{r-2} \cos jx_{r-2}) \\ + (2\mu_j/r)(y_1 \cos jx_1 + y_3 \cos jx_3 + \dots + y_{r-1} \cos jx_{r-1}) \\ (j = 1 \sim r/2) \quad (\text{A3.10})$$

$$b_j = (2\lambda_j/r)(y_0 \sin jx_0 + y_2 \sin jx_2 + \dots + y_{r-2} \sin jx_{r-2}) \\ + (2\mu_j/r)(y_1 \sin jx_1 + y_3 \sin jx_3 + \dots + y_{r-1} \sin jx_{r-1}) \\ (j = 1 \sim r/2-1) \quad (\text{A3.11})$$

and

$$\lambda_0 = 2/3, \quad \mu_0 = 4/3 \quad (\text{A3.12})$$

$$\lambda_j = \{3 + \cos(2j\pi/r')\} / (j\pi r') - \{2 / (j\pi/r')^3\} \sin(2j\pi/r') \quad (\text{A3.13})$$

$$\mu_j = \{4 / (j\pi/r')^3\} \sin(j\pi/r') - \{4 / (j\pi/r')^2\} \cos(j\pi/r') \\ (j = 1 \sim r/2), \quad r' = r/2 \quad (\text{A3.14})$$

A reproducing wave form can be obtained as a series using the following reproducing multiplier α_j .

$$\alpha_j = 1 / \{1 - \cos(2j\pi/l)a\} \quad (\text{A3.15})$$

Accordingly, the coefficients for the new series are:

$$a_0' = a_0 \quad (\text{A3.16})$$

$$a_1' = a_1 / \{1 - \cos(2\pi/l)a\}$$

$$a_2' = a_2 / \{1 - \cos(4\pi/l)a\}$$

...

$$a_{r/2}' = a_{r/2} / \{1 - \cos(r\pi/l)a\} \quad (\text{A3.17})$$

$$b_1' = b_1 / \{1 - \cos(2\pi/l)a\}$$

$$b_2' = b_2 / \{1 - \cos(4\pi/l)a\}$$

. . .

$$b'_{r/2-1} = b_{r/2-1} / [1 - \cos\{(r-2)\pi/l\}a] \quad (\text{A3.18})$$

The new points are:

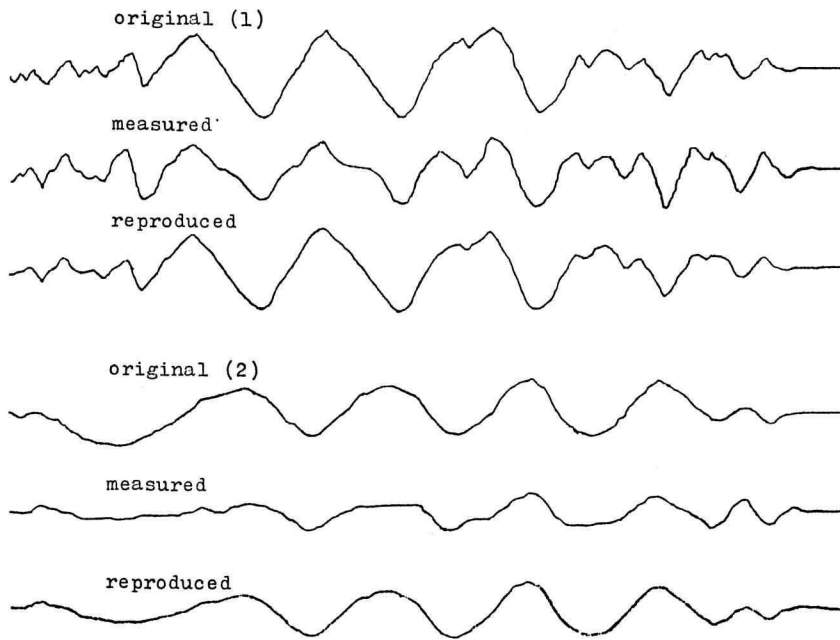


Fig. A3.2 Original, measured and reproduced wave forms

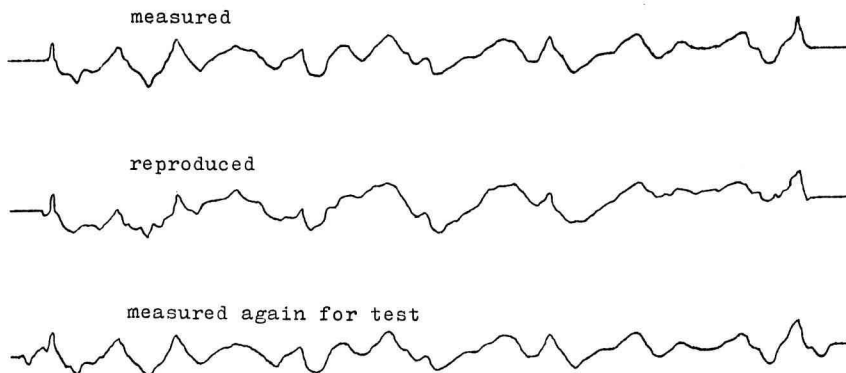


Fig. A3.3 Actual wave forms measured, reproduced, and measured again for checking

$$\begin{aligned}
y_i' = & a_0' + a_1' \cos x_i + \cdots + a_{r/2}' \cos (r/2)x_i \\
& + b_1' \sin x_i + b_2' \sin 2x_i + \cdots + b_{r/2-1}' \sin (r/2-1)x_i \\
& (i = 0 \sim r-1)
\end{aligned} \tag{A3.19}$$

The value of α_j (A3.15) changes $1/2 \sim \infty$, and an upper limit is chosen in practical calculation.

The measured wave form is read with a curve reader or a curve tracer, and expressed with discrete points in digital. A digital computer reads the data tape and makes an original wave form. The results are checked by plotting on x - y recorder as in Fig. A3.2.

The produced original wave form is measured by calculation as similar way of Maya measurement and the obtained wave form is compared to the original measured wave form to judge whether it is good or not. Figure A3.3 is an example of produced original wave form and remeasuring one. Coincidence of measured form and re-measured one concludes that the produced original wave form is almost same as the original one. Here, 2.0 is adopted as the upper limit of α_j , and if this limit is set too high, the error enlargement would become significant.

References

- 1) S. Arai, M. Matsuo: "Simulation of a 2-axle-car Derailment" Railway Technical Research Report, No. 910, RTRI, Japanese National Railways, Jul. 1974 (in Japanese)
- 2) S. Arai: "Simulation of Railway Car Motion" Simulation Technique (II), CORONA Co. 1978 P162~178 (in Japanese)